International journal of scientific and technical research in engineering (IJSTRE)
www.ijstre.com Volume 2 Issue 7 ǁ July 2017.

Rough Wall Kolmogorov Length-Scale Proposal

U. Goldberg
Metacomp Technologies, Inc., Agoura Hills, CA 91301, USA

***Abstract*:** *While the computed transported turbulence dissipation rate, ε, works well as part of a differential equation-based turbulence model in predicting turbulent flows, it doesn't seem to work well when used to determine the Kolmogorov length-scale (ℓ_{Kol}) which, like the other Kolmogorov scales, exists within the viscous sublayer portion of the inner turbulent boundary layer zone. Using ε may lead to an increase in ℓ_{Kol} as roughness increases, the opposite of what should happen. It is proposed here to replace the computed ε (and its level at the 1st point off the wall as dictated by wall functions) with the one resulting from basic law-of-the-wall sublayer relationships which includes the Prandtl-Schlichting (P-S) roughness effect. This approach enables physically correct prediction of ℓ_{Kol}, particularly a reliable decrease thereof with increasing roughness level.*

Keywords: Kolmogorov scales, roughness, viscous sublayer.

I. Introduction

The Kolmogorov length-scale (ℓ_{Kol}), under high Re conditions, is commonly expressed as $(\nu^3/\varepsilon)^{1/4}$ but the computed decay rate of turbulence kinetic energy, ε, doesn't seem to be adequately sensitive to surface roughness, leading to over-estimation and sometimes even wrong behavior of ℓ_{Kol}.This could be a consequence of both the ε transport equation and its wall boundary condition lacking correct roughness effects, even though ε_1 is set by the law-of-the-wall including roughness effect.

An alternative way to express ℓ_{Kol} is proposed here, its basic formulation being desensitized to whether the first off-wall computational points lay within the viscous sublayer (including the solve-to-wall level of $y^+ \leq 1$) or in the logarithmic overlap (see Appendix for flow property details in these regions).The basic aim is to select formulation ingredients such that the resulting ℓ_{Kol} is minimal (to admit more small roughness levels) and sensitive to the roughness size since surface (boundary) conditions are strongly influencing the immediately adjacent viscous sublayer where Kolmogorov micro-scales are defined. Effect of roughness height on boundary layer features is seen below:

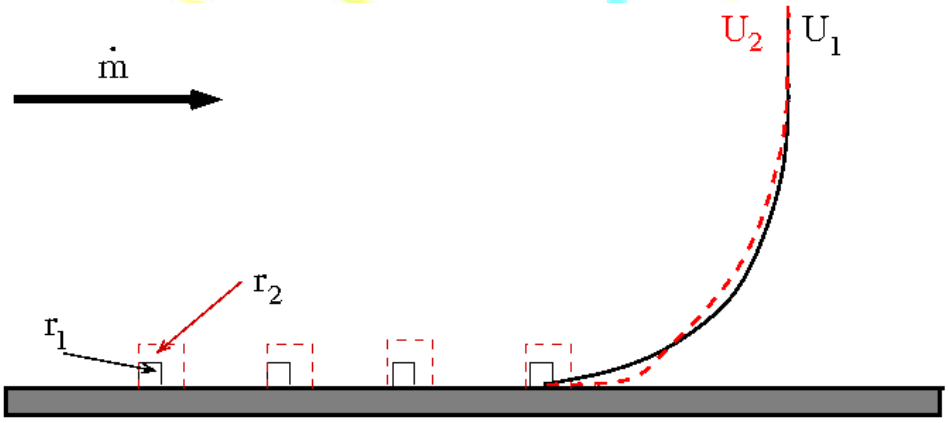

Figure 1. Velocity profile vs. roughness height

As seen in Fig. 1, the larger roughness element, r_2, causes increase in τ_w (red broken line velocity profile, U_2) but the outer velocity portion of U_2 is the same as that of the smaller roughness, r_1. Conservation on mass-flow-rate, $\dot{m}$, dictates adjustments within the lower section of the boundary layer. Thus the inner portion of the boundary layer (viscous sublayer and logarithmic overlap) shrinks in the normal-to-wall direction, whence the dissipative eddies become smaller. And since ℓ_{Kol} is a measure of these eddies, it is expected to also become smaller as the roughness increases.

Following the next Theory section, five examples are given to exhibit the usefulness of the proposed approach to compute ℓ_{Kol}.

Theory

1. Definition of ℓ_{Kol}

Following Eq. (C1) in the Appendix,

$$\varepsilon = \frac{2A_\varepsilon k^2}{\nu R_y(1-e^{-A_\varepsilon R_y})} \tag{1}$$

where

$$A_\varepsilon = C_\mu^{3/4}/(2\kappa) \tag{1a}$$

$$R_y = min\{y^+/C_\mu^{1/4}, \sqrt{A_k}y^{+^2}\}, \quad A_k \cong 0.0266 \tag{1b}$$

Here the 2nd term within the parentheses represents the viscous sublayer. Thus

$$\ell_{Kol} = \left(\frac{\nu^3}{\varepsilon}\right)^{1/4} = \frac{\nu}{\sqrt{k}}\left[\frac{R_y(1-e^{-A_\varepsilon R_y})}{2A_\varepsilon}\right]^{1/4} \tag{2}$$

where k (see Appendix Eq. (A1) and Fig. 2) is chosen at its maximum value, attained within the logarithmic layer:

$$k = \frac{1}{\sqrt{C_\mu}}\left(\frac{|\tau|}{\rho}\right)_w \tag{3}$$

Importantly, τ_w magnitude increases with roughness size, thereby increasing k and, by Eq. 2, decreasing ℓ_{Kol}. This is concluded also for the original $\ell_{Kol} = \left(\frac{\nu^3}{\varepsilon}\right)^{1/4}$ based on the behavior of ε within the viscous sublayer, leading to $\ell_{Kol} = \left(\frac{\nu^3}{\varepsilon}\right)^{1/4} = (2A_k)^{-1/4}\nu\sqrt{\left(\frac{\varrho}{\tau}\right)_w}$. Fig. 3 shows experimental data (Bellucci et al., 2014) of increasing k with roughness level in the viscous sublayer. Since $\varepsilon \sim k^2/\nu$ within the sublayer, ε also gets larger with increasing roughness. Consequently, both original and proposed ℓ_{Kol} will be reduced in size as roughness increases. This has been found also in Marati et al., 2004, where $\ell_{Kol} = \frac{(\kappa y)^{1/4}\nu^{3/4}}{(\tau_w/\rho_w)^{3/8}}$.

The effect of roughness on τ_w is based on the P-S (Prandtl and Schlichting, 1934) skin friction formula when the 1st computational points are within the viscous sublayer:

$$C_f = \left(2.87 + 1.58log_{10}\frac{s}{K_S}\right)^{-2.5} / \left(1+\frac{\gamma-1}{2}M_\infty^2\right)^{0.467}, \tau_w = -\frac{1}{2}\varrho_\infty U_\infty^2 C_f \text{ and } u_\tau = \sqrt{(\tau/\rho)_w} \tag{4}$$

This is combined with equations 2 and 3, thus introducing roughness effect explicitly.

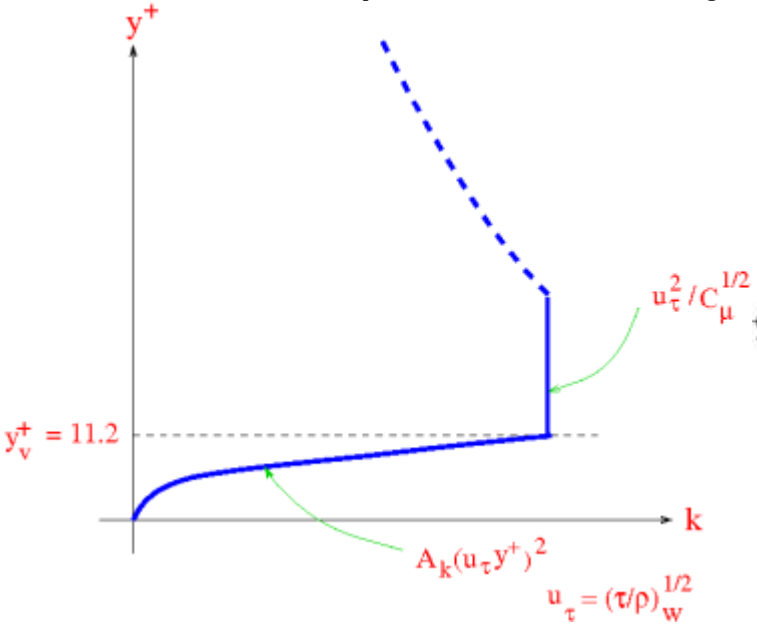

Figure 2. Sketch of near-wall profile of k

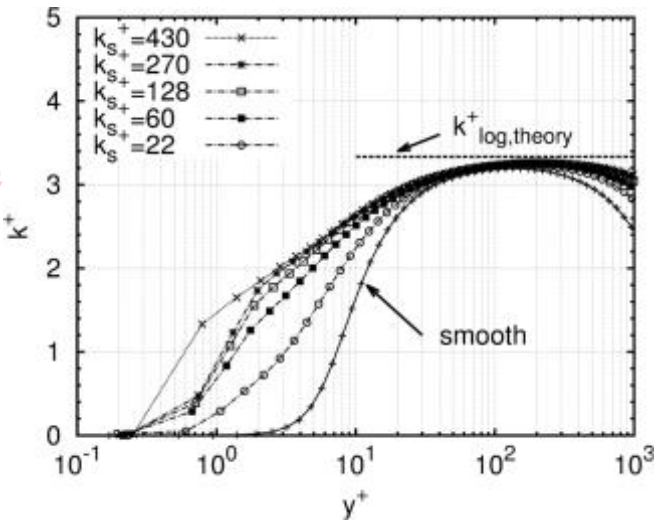

Figure 3. Sublayer increase of k with roughness, from Ref. [1]

2. The Kolmogorov length-scale as a function of s

Based on the Appendix Eqs. (B7-B8), the Kolmogorov length-scale grows along the surface streamline distance, s, as follows:

$$\ell_{Kol_{sublayer}} \sim \sqrt{(\rho/\tau)_w} = \frac{1}{\sqrt{\nu_w (\partial u/\partial y)_w}} \quad (5a)$$

$$\ell_{Kol_{log-layer}} \sim \left[\frac{\nu}{\sqrt{(\tau/\varrho)_w}}\right]^{1/4} = \left[\frac{\nu/\nu_w}{(\partial u/\partial y)_w}\right]^{1/4} \quad (5b)$$

and since $(\partial u/\partial y)_w$ commonly becomes smaller along s, the Kolmogorov length-scale grows along it as seen in Fig. 4.

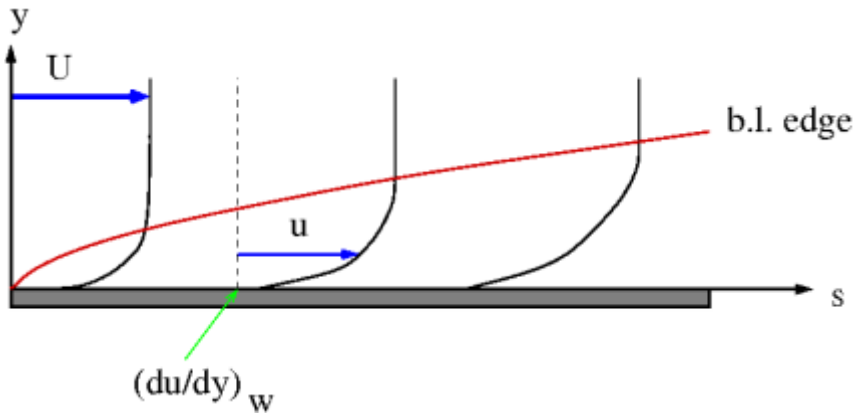

Figure 4. $(\partial U_t/\partial y)_w$ diminishes along the streamwise direction

Test cases

The commercial flow solver CFD++ (see details in Chakravarthy, 1999) was used with the realizable k-ε closure (Goldberg et al., 1998) to compute the following flow examples, using a non-equilibrium wall function (see Appendix) which includes the effects of $\partial p/\partial s$ and roughness, the latter by Eq. (4). All grids used for the following flow cases have been previously established to yield mesh-independent solutions.

(I) Flat plate

Air flow over a rough plate was computed with two roughness levels: K_S=3 micro (μ)-meter and 0.6 mm. 1st off-plate grid centroids were once within the viscous sublayer (y*=7) and once in the logarithmic layer (y*=56). Fig. 5 compares ℓ_{Kol} based on the standard, directly computed ε, $(\nu^3/\varepsilon)^{1/4}$, with that based on Equations 1-4. The choice of $K_S = 3x10^{-6}$ m emanates from Schlichting 1968, p.612, where camouflage paint of this equivalent sand-grain height was applied to a war plane, resulting in a substantial increase in friction drag relative to that of the unpainted airplane. The standard Kolmogorov length-scale is about 5 times larger than this Ks, rendering it negligible even though in reality it has a large effect on viscous drag. This indicates that the standard ℓ_{Kol} formula may not be adequate for cases involving rough surfaces, suggesting the alternative formulation hereby proposed. The standard formula predicts a considerably larger drop in ℓ_{Kol} than the proposed method does as the K_S magnitude increases to 0.6 mm (solid vs. dashed lines in Fig. 5L). A similar trend is observed in the y^+=56 case (Fig. 5R), however, since the Kolmogorov scales exist only within the viscous sublayer, the 1st computational point must be inside this sublayer, therefore y^+=56 is not acceptable. Since the smaller ℓ_{Kol} is predicted by the current proposal, it admits a larger range of roughness sizes. This test case indicates that limiting the 1st off-surface computational points within the viscous sublayer (including $y^* \leq 1$ for direct solve-to-wall) is the preferable approach (Fig. 5L) which adheres to the physics since the Kolmogorov scales exist only within the viscous sublayer.

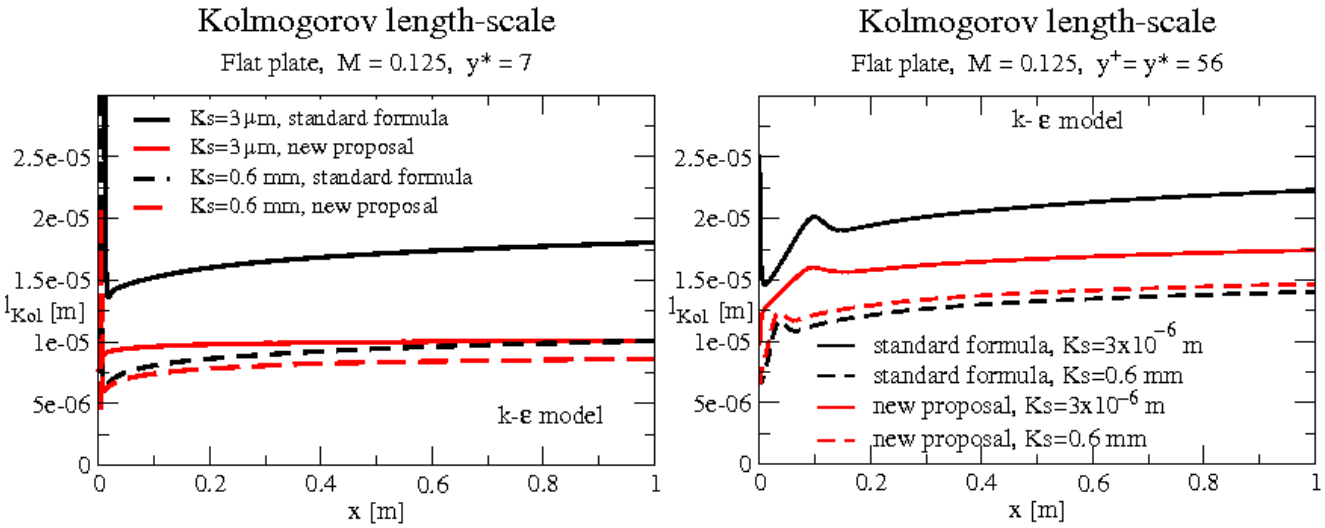

Figure 5. ℓ_{Kol} profiles along a rough plate, K_S=3μm and 0.6 mm.1st computational points being inside the viscous sublayer(L) and within the logarithmic layer (R)

(II) Flow over a curved surface

This is a case of flow over a curved surface (from Suga et al., 2006). Wall geometry and computational mesh are shown in Fig. 6(L), consisting of 4672 cells of which 2426 are triangles and the rest are quadrilaterals adjacent to the wall. 91 cells are along the wall and 50 normal to it, of which 23 are the quadrilaterals. The 1st row along the wall has a 0.5 mm height, corresponding to y*≅ 10 upstream of the curve and y*≅ 8 along it. The wall is subject to air flow at a temperature of 288 K and U_∞=22 m/s.

Figure 6(R) shows ℓ_{Kol} profiles along the wall for rough surfaces with K_S=0.003 mm and 0.6 mm. As in the flat plate case, Eq. (2) predicts lower ℓ_{Kol} levels than those from the standard approach, thereby widening the range of admissible small K_S levels. Both methods predict lower levels of ℓ_{Kol}under the higher roughness level as expected.

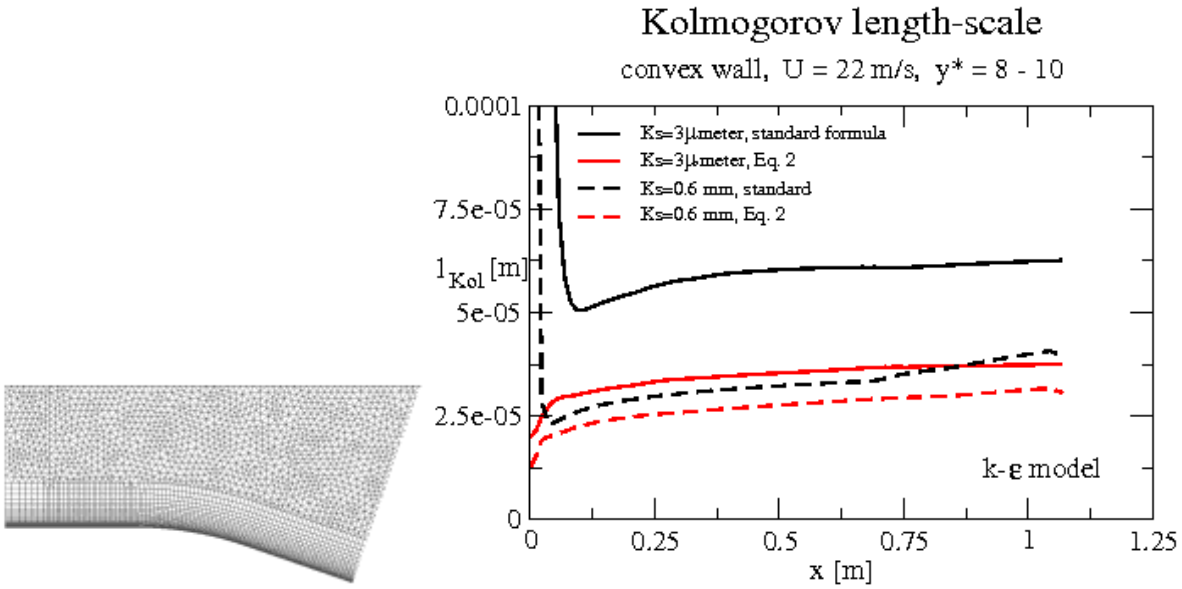

Figure 6. (L) Computational domain, (R) ℓ_{Kol}profiles

It is noted in both the above examples (as well as in the next ones) that the leading-edge zone of the surface exhibits very large ℓ_{Kol} as predicted by the standard method, $\ell_{Kol} = (\nu^3/\varepsilon)^{1/4}$, likely due to underprediction of ε in that region, whereas the proposed approach (Equations 1-4) behaves considerably better in this zone.

(III) NACA 0012 airfoil at α=6º

Addressed in Lu and Liou, 2009, this airfoil mesh has 113362 triangles and 12680 quadrilaterals. There are 947 quadrilateral cells around the airfoil with y*≅5 in the trailing edge region on both pressure and suction sides and y*≅ 15 in the leading-edge zone (Fig. 7L).

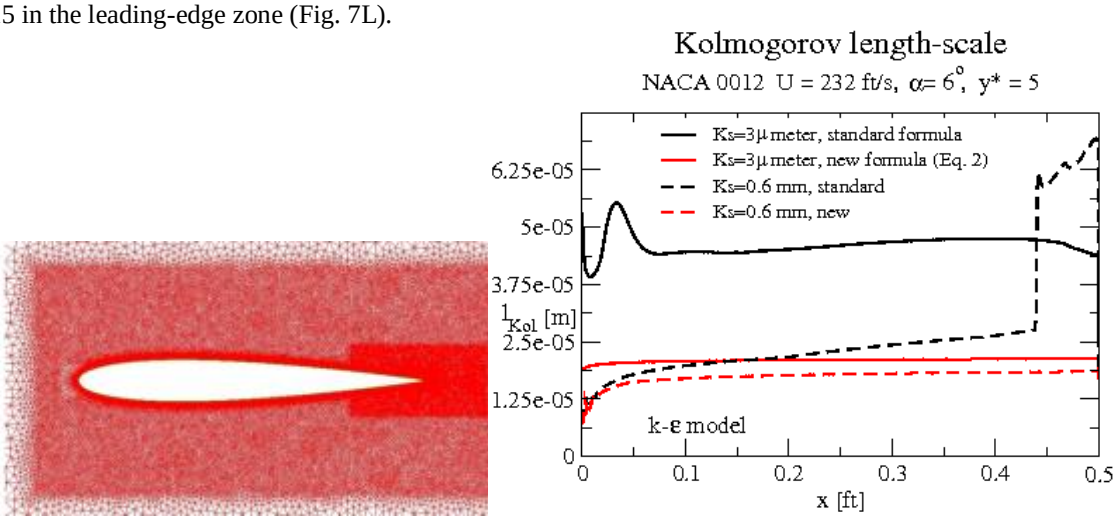

Figure 7. (L) mesh around the airfoil, (R) ℓ_{Kol}profiles along the NACA 0012 suction surface.

As in previous cases, the proposed formulation yields a smaller ℓ_{Kol}than the standard one does and in this case also produces no oscillation at the leading-edge zone (Fig. 7R), as opposed to the standard approach. Comparing the 0.6 mm rough wall results with those of the 3 μ-meter one shows the consistency of the proposed approach versus the inconsistency of the standard one regarding the behavior of $\ell_{Kol}$when switching from lower to higher roughness: Along the trailing edge section ℓ_{Kol} is predicted larger for the higher roughness whereas the opposite is physically correct. On the other hand, the proposed method (red lines) is consistently correct along the entire airfoil.

(IV) Water flow over a sand dune

This test case is a sand dune with water flowing over it (from Suga et al., 2006). The flow includes a separation zone at the bottom of the dune. Equivalent sand-grain roughness heights of 3 μ-meter and 0.6 mm are compared as before. The domain is 1.6 m long and the free air/water surface is located 0.292 m above the level of the beginning of the dune, treated as a symmetry boundary to prevent flow normal to it. The bulk mean velocity is U = 0.633 m/s and the Reynolds number, based on U and the free surface height, is 175,000. The quadrilaterals grid size is 16,121 and the 1st computational points above the dune are within the viscous sublayer, y*=7 being a typical level. Figure 8(L) shows the grid and 8(R) shows plots of ℓ_{Kol}profiles along the dune for the two roughness levels, as predicted by the standard and proposed formulations.

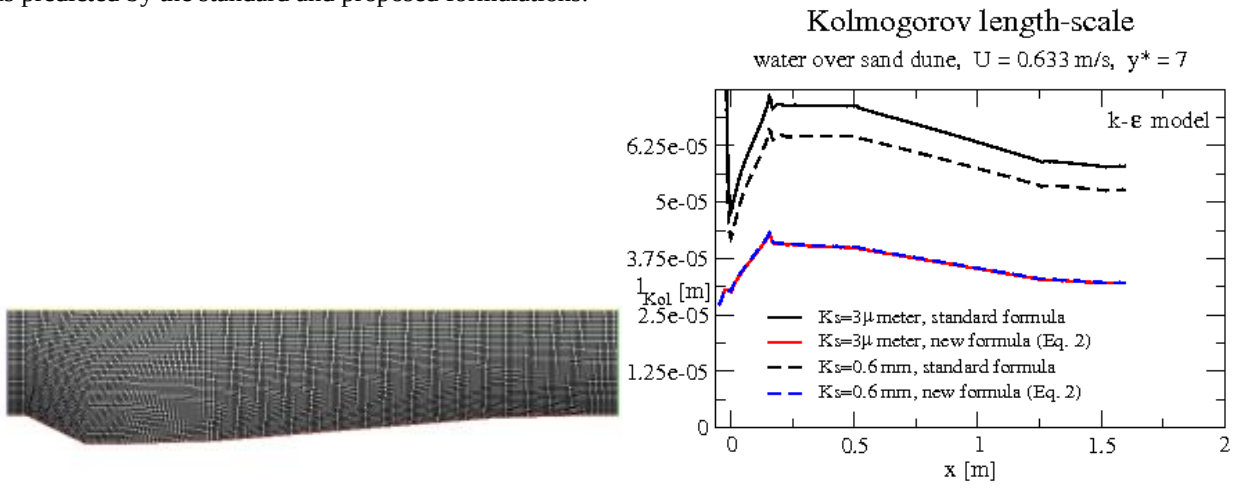

Figure 8. (L) Sand dune mesh, (R) ℓ_{Kol}profiles along dune (lower surface)

It is noticed in Fig. 8R that the proposed ℓ_{Kol} shows no difference in spite of a factor of 200 between the two roughness levels. The reason is the high density of water. For example, at the mid-point (x=0.8 m) the two levels

of roughness give rise (Eq. 3) to $\Delta k = \frac{\Delta\tau_w}{\rho_w} = \frac{0.031}{1003.9} \cong 3 \times 10^{-5}(\text{m/s})^2$ and that imposes a negligible change in ℓ_{Kol}, Eq. 2. However, like in previous examples, the new ℓ_{Kol} is smaller than the one from the standard approach and it doesn't suffer from over-predicting ℓ_{Kol} in the inlet zone as the standard method does.

(V) Channel flow with a lower rough wall including a curved portion

Here is a channel flow with a rough lower surface which includes a curved portion. Song and Eaton, 2002, describe this flow case. Figures 9 show topology and grid for this case. Fig. 9(L) includes details like the circular curved ramp section length of L=70 mm, its radius of 127 mm and its 21 mm height. The mesh is especially dense in the curved ramp area due to the flow being separated there. The upper channel wall is smooth while the lower wall is rough (originally with K_S=1.2 mm but here K_S=3 μ-meter and 0.6 mm are used). Inflow speed is 20 m/s and turbulence levels are Tu=0.5% and μ_t/μ=30. The 11,200 cells mesh has 8,000 quadrilaterals and the rest are triangles. The 0.15 mm height of the next-to-walls grid layer translates into $7 \geq y^* \geq 4$ on the ramp wall.

Fig. 10 compares ℓ_{Kol} along the lower surface for K_S=0.6 mm and K_S=3 μ-meter levels of roughness, using both standard and new methods. Both approaches reduce ℓ_{Kol} as the roughness increases, with the standard method producing a considerably larger jump as in previous cases. However, the proposed method predicts a smaller ℓ_{Kol} level for the 3 μ-meter roughness than the standard one predicts for the 0.6 mm roughness (a trend seen in previous flow examples) and, as before, it avoids the standard method's trend of overpredicting ℓ_{Kol} in the inlet region.

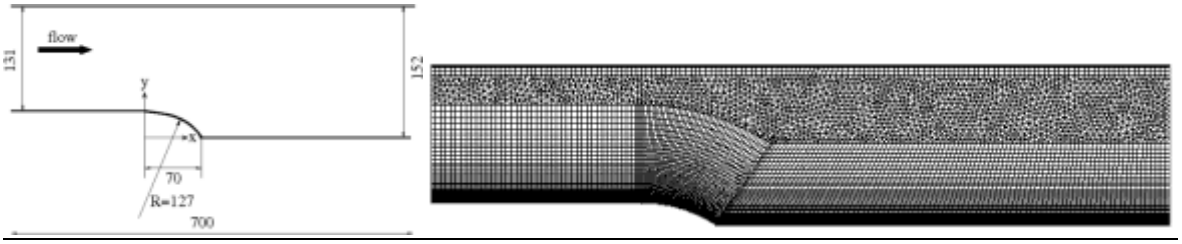

Figure 9. (L) Topology and dimensions, (R) Grid

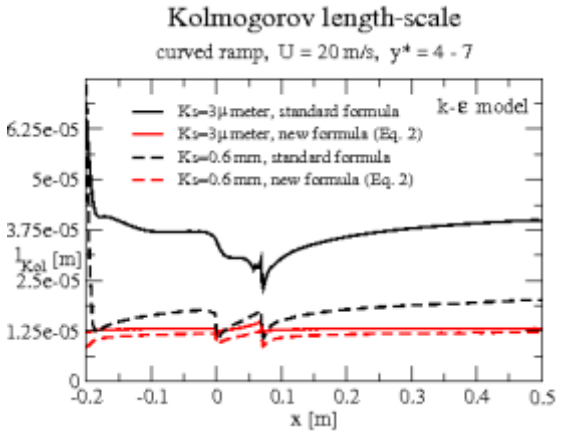

Figure 10. ℓ_{Kol} profiles along curved ramp (lower surface)

Concluding observations

(1) The larger the roughness, the thinner the inner boundary layer - including the sublayer, due to increased $(\partial U_t/\partial y)_w$ (Fig. 1). That translates into *smaller* dissipative eddies. Since ℓ_{Kol} is a measure of these eddies within the sublayer, it is also expected to shrink in size with increasing roughness. The proposed approach adheres to this: ℓ_{Kol} decreases when moving from a low roughness level to a higher one (examples 1, 2, 3 and 5). However, the standard method predicts the opposite trend in the trailing edge region of example 3 (airfoil), this being unphysical. On the other hand, in examples1, 2, 4 and 5 the standard method does predict the correct trend.

(2) When switching from $K_{S,1}$= 3 μ-meter to $K_{S,2}$= 0.6 mm roughness, a change in ℓ_{Kol} of $\frac{\ell_{kol,1}}{\ell_{kol,2}} \simeq \left(\frac{2.87+1.58log_{10}\frac{s}{K_{S,1}}}{2.87+1.58log_{10}\frac{s}{K_{S,2}}}\right)^{1.25}$ is expected, based on Eqs (2-4). With s=1 m this ratio is about 1.6. In the1st example the standard method yields 1.8 and the new one gives 1.2. In the 2nd one the standard method predicts 1.6 while the proposed one yields again 1.2. In the 5th case 2.0 results from the standard approach whereas the new one predicts a ratio ≈1. Thus, the standard method is closer to the expected ratio, however, it exhibits a wrong-oriented ratio in example 3.

(3) Again, in the 3rd example (airfoil), along the trailing edge zone, the standard method predicts that the rougher wall causes a large *increase* in ℓ_{Kol} whereas the opposite is correct, based on fundamental near-wall relationships from the law-of-the-wall in the viscous sublayer (Equations1-4 and the Appendix). Along the rest of the airfoil the standard method does recover the correct behavior, but the proposed approach maintains correct prediction trends along the *entire* airfoil.

(4) The standard approach introduces high levels of ℓ_{Kol} in the inflow (or leading edge) region, as seen in cases 1, 2, 4 and 5. The new method doesn't suffer from this phenomenon due to avoiding usage of the solved variable ε.

(5) The proposed method is based on the fundamental rules of the sublayer's wall function (Equations 1-3 which already include roughness effects by using the P-S [Prandtl and Schlichting, 1934] skin friction formula, Eq. 4) and those rules have been proven correct since many years ago, based on numerous experimental data. Since there is no such thing as a truly smooth surface, wall functions have long been valid for mildly rough walls as long as roughness is taken into account in the form of a sand-grain equivalent height, without changing the surface geometry. Of course, large roughness (e.g. K_S > 3 mm) should be implemented as part of the surface geometry and grid, in which case the currently proposed treatment isn't necessary.

(6) Whenever there are doubts, it is always advantageous to resort to fundamental relationships. In the present case eliminating ε, computed from its own transport equation and subject to its own wall BC (with $\varepsilon_1 = 2A_k u_\tau^4/\nu$, see Appendix B, and P_k=0 in the viscous sublayer) and replacing ε with the fundamental wall function-based description thereof (Equations 1-3 which include the P-S roughness-influenced C_f, Eq. 4) is a safe and secure way of dealing with ℓ_{Kol}.

Nomenclature

A_k=0.0266, constant used in the viscous sublayer
B ≅ 5.5, constant in the logarithmic wall function branch
C_f skin friction
C_μ=0.09, coefficient of eddy viscosity in some k-ε turbulence models
E=9.8, constant in some forms of the logarithmic Law-of-the-Wall
f_μ near-wall damping function
K_S sand grain height representing roughness level
k turbulence kinetic energy
ℓ length-scale
M Mach number
P_k production of turbulence kinetic energy
p static pressure
Re flow Reynolds number
R_t turbulence Reynolds number
R_y turbulence Reynolds number based on y^+
S strain rate
s distance along body contour
Tu freestream turbulence intensity
U, u streamwise velocity component
U_t tangent-to-wall velocity component
$u^+=U_t/u_\tau$, non-dimensional speed for wall functions
$u_\tau=(|\tau|/\rho)_w^{1/2}$, friction speed
y normal-to-surface distance
$y^+=yu_\tau/\nu$, normal-to-wall dimensionless coordinate for wall functions
$y^*=C_\mu^{1/4}\sqrt{k}y/\nu$, k-based normal-to-wall dimensionless coordinate for wall functions

Greek letters

ε dissipation rate of turbulence production

$\gamma = C_p/C_v$,	specific heat ratio
$\kappa \cong 0.41$,	von Karman constant
μ	dynamic molecular viscosity
μ_t	dynamic eddy viscosity
$\nu = \mu/\rho$,	kinematic molecular viscosity
$\nu_t = \mu_t/\rho$,	kinematic eddy viscosity
ρ	density
τ	shear stress
subscripts	
1	denoting 1st off-wall computational point
∞	freestream conditions
c	corrected for compressibility effects
Kol	of Kolmogorov
t	turbulent or tangential
w	at wall

References

[1.] Bellucci, J., Rubechini, F., Marconcini, M. and Arnone, A., "The Influence of Roughness on a High-Pressure Steam Turbine Stage: An Experimental and Numerical Study", *J. Eng. Gas Turbines Power* **137**(1), 2014.

[2.] Chakravarthy, S., "A Unified-Grid Finite Volume Formulation for Computational Fluid Dynamics," *Int. J. Numer. Meth. Fluids*, **31**, pp.309-323, 1999.

[3.] Goldberg, U., Peroomian, O. and Chakravarthy, S., "A Wall-Distance-Free k-ε Model with Enhanced Near-Wall Treatment," *J. Fluids Eng*., **120,** pp.457-462, 1998.

[4.] Lu, M-H and Liou, W., "Numerical Study of Roughness Effects on a NACA 0012 Airfoil Using a New Second-Order Closure of the Rough Wall Layer Modeling," *AIAA 2009-52*, 47th AIAA Aerospace Sciences Meeting, Orlando, January 2009.

[5.] Marati, N., Casciola, C.M. and Piva, R., "Energy cascade and spatial fluxes in wall turbulence," *J. Fluid Mech*., **521**, pp.191-215, 2004.

[6.] Prandtl, L. and Schlichting, H., *Werft, Reederei, Hafen*, **1934**: 1-4, 1934.

[7.] Schlichting, H., "Boundary Layer Theory", 6th Ed., McGraw-Hill Co., 1968.

[8.] Song, S. and Eaton, J.K., "The effects of wall roughness on the separated flow over a smoothly contoured ramp," *Exp. Fluids* **33**, 38-46, 2002.

[9.] Suga, K., Craft, T. and Iacovides, H., "An analytical wall-function for turbulent flows and heat transfer over rough walls," *Int. J. of Heat and Fluid Flow*, **27**, pp.852–866, 2006.

Appendix: BASIC SUBLAYER/LOG-LAYER RELATIONSHIPS

A. Logarithmic layer

$$k = u_\tau^2/\sqrt{C_\mu}\,,\ u_\tau = \sqrt{(\tau/\rho)_w} \tag{A1}$$

$$\varepsilon = u_\tau^3/(\kappa y) \tag{A2}$$

$$\nu_t = \kappa y u_\tau \tag{A3}$$

$$S = u_\tau/(\kappa y) \tag{A4}$$

Kolmogorov velocity scale: $(n\varepsilon)^{1/4} = \sqrt{ky}\left(nS^3\right)^{1/4}$ (A5)

Realizable time-scale: $T_t = \frac{k}{\varepsilon} = \frac{\kappa y}{u_\tau \sqrt{C_\mu}}$ (A6)

$$R_y = y^+ / C_m^{1/4} \tag{A7}$$

$$R_t = C_\mu^{-3/4} \kappa \mathrm{R_y} \tag{A8}$$

$$u^+ = ln\left(e^B y^{+^{1/\kappa}}\right), \qquad B = 5.5, \qquad \kappa = 0.41 \tag{A9}$$

The above assumes that f_μ=1 in the expression $\nu_t = C_\mu f_\mu k^2/\varepsilon$.

B. Viscous sublayer

$$u^+ = y^+ \tag{B1}$$

$$y^+ = \sqrt{\frac{y}{\nu}}\left(\frac{k}{A_k}\right)^{1/4}, \qquad A_k \cong 0.0266 \tag{B2}$$

$$k = A_k(u_\tau y^+)^2 = A_k u^2 \tag{B3}$$

$$\varepsilon = \frac{2A_k u_\tau^4}{\nu} \tag{B4}$$

$$\nu_t = C_\mu A_\mu \frac{A_k}{\sqrt{2}} \nu y^{+^4}, \quad A_\mu \cong 0.0084 \tag{B5}$$

$$S = \frac{u_\tau^2}{\nu} \tag{B6}$$

Kolmogorov velocity scale: $(\nu\varepsilon)^{\frac{1}{4}} = (2A_k)^{\frac{1}{4}}\sqrt{\nu S} \cong 0.48\sqrt{\nu S} = \left(\frac{A_k}{2}\right)^{\frac{1}{4}} U_\infty \sqrt{C_f} \cong 0.34 U_\infty \sqrt{C_f}$ (B7)

Realizable time-scale: $T_t = \frac{1}{\sqrt{A_k}} \frac{\nu}{u_\tau^2}$ (B8)

$$R_y = \sqrt{A_k} y^{+^2} \tag{B9}$$

$$R_t = \frac{A_k}{2} y^{+^4} = \frac{R_y^2}{2} \tag{B10}$$

C. General ε formula (based on the above)

$$\varepsilon = 2A_\varepsilon \frac{k^2}{\nu R_y (1 - e^{-A_\varepsilon R_y})} \tag{C1}$$

$$A_\varepsilon = \frac{C_\mu^{3/4}}{(2\kappa)} = 0.2 \tag{C2}$$

$$R_y = min\left\{C_\mu^{-1/4} y^+, \sqrt{A_k} y^{+^2}\right\} \tag{C3}$$

or

$$R_y = max\left\{\sqrt{2R_t}, 2A_\varepsilon R_t\right\} \tag{C4}$$